Image Recovery via Truncated Weighted Schatten-p Norm Regularization

Lei Feng[1(✉)] and Jun Zhu[1,2]

[1] Jinling Institute of Technology, Nanjing 211169, China
fenglei492327278@126.com
[2] Nanjing University of Science and Technology, Nanjing 210094, China

Abstract. Low-rank prior knowledge has indicated great superiority in the field of image processing. However, how to solve the NP-hard problem containing rank norm is crucial to the recovery results. In this paper, truncated weighted schatten-p norm, which is employed to approximate the rank function by taking advantages of both weighted nuclear norm and truncated schatten-p norm, has been proposed toward better exploiting low-rank property in image CS recovery. At last, we have developed an efficient iterative scheme based on alternating direction method of multipliers to accurately solve the nonconvex optimization model. Experimental results demonstrate that our proposed algorithm is exceeding the existing state-of-the-art methods, both visually and quantitatively.

Keywords: Compressive sensing
Truncated weighted schatten-p norm
Alternating direction method of multipliers

1 Introduction

Compressive Sensing (CS) [1–5] draws recently much more attention in the field of image processing. Compared with the traditional scheme of sampling followed by compressing, CS carries out the above two steps at the same time. From fewer measurements than required by Nyquist theorem, CS can efficiently reconstruct images under the condition that they satisfy the sparsity.

Traditional CS algorithms often exploit the sparsity in some transform domains [6–11]. Lately, the intrinsic low-rank property exploited by self-similarity and nonlocal operation, has widely used in many research fields, such as face recognition [12–14], image inpainting [15] and compressive sensing [16,17]. These methods based on low-rank property have shown competitive performances in each area.

The success of these low-rank regularization based CS methods depends on the solution of the low-rank regularization problem. Unfortunately, the low-rank regularization problem is NP-hard and there is no method to solve it directly. Many methods use different substitution functions to approximate the rank function [18–20]. [18,19] selected convex nuclear norm and employed singular value

thresholding [21] to efficiently resolve the rank regularization problem. Compared with the original rank definition has the fact that all nonzero singular values play the same important role, the nuclear norm based approaches minimized the summarization of all the singular values. [16] chose logdet function (the logarithm sum of all the singular values) and can obtain better results than nuclear norm. However, logdet function is fixed and essentially deviates from the rank function. In order to obtain a competitive solution of low-rank regularization problem, many methods adopt distinct schemes and treat each singular value differently [22–25]. Weighted nuclear norm [22] assigned larger weights to larger singular values and smaller weights to smaller ones. So smaller singular values are penalized more than larger ones. Since the largest r (the rank) singular values will not impact the rank, in our previous work, truncated schatten-p norm [24] abandoned them and only minimized the summation of surplus singular values to the power of p.

In this paper, truncated weighted schatten-p norm (TWSP), which is taking advantages of both weighted nuclear norm and truncated schatten-p norm, has been firstly proposed toward better exploiting low-rank property in image CS recovery. At last, we further propose an efficient iterative scheme based on alternating direction method of multipliers to accurately solve the nonconvex optimization model.

The reminder is organized as follows. Section 2 simply reviews the weighted nuclear norm based image CS model and truncated schatten-p norm based image CS model. In Sect. 3, our proposed TWSP and an efficient iterative scheme for the optimization model are given in details. In Sect. 4, the effectiveness of our method is proved by several experiments. Finally, we summarize our proposed model in Sect. 5.

2   Related Work

In this section, we will review low-rank regularization based image CS recovery model. Suppose an image is defined as $x \in R^n$ and its sampling matrix is $\Phi \in R^{m \times n}(m \ll n)$, the purpose of CS is to reconstruct the image x from the measurement $y \in R^m$ ($y = \Phi x$) than suggested by traditional Nyquist sampling theorem.

Usually, natural images have a large number of repetitive structures and these blocks with repetitive structures are located in the global scope of the images. So the rank of each block matrix grouped by corresponding nonlocal similar blocks is low. The intrinsic low-rank property exploited by self-similarity and nonlocal operation, has widely used in face recognition, compressive sensing and image denoising. These methods based on low-rank property have shown competitive performances in each area.

Suppose $x_j \in R^d$ is a block, we query for h most similar blocks from all image blocks. $R_j x = [R_{j_1} x, R_{j_2} x, \cdots R_{j_h} x] \in R^{d \times h}$ (R_{j_k} is the corresponding extraction matrix) is the j-th block matrix formed by these similar blocks. Then the CS recovery problem is formulated as follows:

$$(x, L_j) = \arg\min_{x, L_j} \|y - \Phi x\|_F^2 + \lambda \sum_j rank\,(R_j x)\,. \tag{1}$$

where $\|\cdot\|_F^2$ is the square sum of all elements.

Weighted nuclear norm [22] assigned larger weights to larger singular values and smaller weights to smaller ones. So smaller singular values are penalized more than larger ones. So the weighted nuclear norm based image CS model is represented as follows:

$$x = \arg\min_x \|y - \Phi x\|_F^2 + \lambda \sum_j \sum_{i=1}^{\min(d,h)} w_i \delta_i\,(R_j x)\,. \tag{2}$$

where $w_i = \rho\sqrt{h}\big/\left(\delta_i\left(A_j^s\right) + \varepsilon\right)$, ρ is a normal number and $\varepsilon = 10^{-16}$.

Since the largest r (the rank) singular values will not impact the rank, truncated schatten-p norm [24] abandoned them and only minimized the summation of surplus singular values to the power of p. Then the truncated schatten-p norm based image CS model is defined as

$$(x, A_j, B_j) = \arg\min_{x, A_j, B_j} \|y - \Phi x\|_F^2 + \lambda \sum_j \sum_{i=1}^{\min(d,h)} \delta_i^p\,(R_j x) \cdot \left(1 - \delta_i\left(B_j^T A_j\right)\right)\,. \tag{3}$$

Assume $U \Delta V^T$ is the singular value decomposition of L_j, where $\Delta \in R^{d \times h}$, $U = (u_1, \ldots u_d) \in R^{d \times d}$ and $V = (v_1, \ldots v_h) \in R^{h \times h}$, then $A \in R^{r \times d}$ and $B \in R^{r \times h}$ are the corresponding transposition of former r columns from U and V respectively.

3 Truncated Weighted Schatten-p Norm for Image Compressive Sensing Recovery

In this paper, to obtain better results of low-rank regularization problem, truncated weighted schatten-p norm regularization, which is taking advantages of both weighted nuclear norm and truncated schatten-p norm, is presented toward better exploiting low-rank property. Specially, we only minimize the summation of few smallest singular values to the power of p multiplied by the certain weights.

From the above analysis, our method can be modeled as

$$(x, A_j, B_j, w_i) = \arg\min_{x, A_j, B_j, w_i} \|y - \Phi x\|_F^2 + \lambda \sum_j \sum_{i=1}^{\min(d,h)} w_i \delta_i^p\,(R_j x)\left(1 - \delta_i\left(B_j^T A_j\right)\right)\,. \tag{4}$$

Except for the compressive measurements, all the other information cannot be known. We introduce auxiliary variables and address the above problem by alternating direction method of multipliers, where the image x, the block group

$R_j x$ and the corresponding auxiliary variable L_j are computed in turn. Then Eq. (4) can be reformulated as

$$(x, A_j, B_j, w_i, L_j) = \underset{x, A_j, B_j, w_i, L_j}{\arg\min} \|y - \Phi x\|_F^2 +$$
$$\lambda \sum_j \left(\sum_{i=1}^{\min(d,h)} w_i \delta_i^p (L_j) \left(1 - \delta_i \left(B_j^T A_j\right)\right) + \beta \|R_j x - L_j\|_F^2 \right). \tag{5}$$

Equation (5) contains the following four subproblems.

$$\left(A_j^{t+1}, B_j^{t+1}\right) = \underset{A_j, B_j}{argmax} \sum_{i=1}^{\min(d,h)} w_i^t \delta_i^p (L_j) \delta_i \left(B_j^T A_j\right). \tag{6}$$

$$w_i^{t+1} = \underset{w_i}{\arg\min} \sum_{i=1}^{\min(d,h)} w_i \delta_i^p (L_j) \left(1 - \delta_i \left(\left(B_j^{t+1}\right)^T A_j^{t+1}\right)\right). \tag{7}$$

$$L_j^{t+1} = \underset{L_j}{\arg\min} \sum_{i=1}^{\min(d,h)} w_i^{t+1} \delta_i^p (L_j) \left(1 - \delta_i \left(\left(B_j^{t+1}\right)^T A_j^{t+1}\right)\right) + \beta \|R_j x^t - L_j\|_F^2. \tag{8}$$

$$x^{t+1} = \underset{x}{\arg\min} \|y - \Phi x\|_F^2 + \lambda\beta \sum_j \left\{ \|R_j x - L_j^{t+1}\|_F^2 \right\}. \tag{9}$$

3.1 $\{A_j, B_j\}$ Subproblem

According to the definition of truncated schatten-p norm [24], when A^{t+1} and B^{t+1} are calculated based on singular value decomposition of L_j^t, Eq. (6) gets the maximal value. Given intermediate estimated value L_j^t, we first calculate the singular value decomposition of L_j^t ($\left[U_j^t, \Delta_j^t, V_j^t\right] = svd(L_j^t)$), and then estimate A^{t+1} and B^{t+1} by the following formula.

$$A^{t+1} = \left(u_{j_1}^t, \ldots u_{j_r}^t\right)^T, \quad B^{t+1} = \left(v_{j_1}^t, \ldots v_{j_r}^t\right)^T. \tag{10}$$

3.2 w_j Subproblem

Since the larger singular values are corresponding to the energy of the major components, they are more important than the smaller ones. According to the definition of weighted nuclear norm [22], we set

$$w_i^{t+1} = \rho\sqrt{h} / \left(\delta_i \left(L_j^t\right) + \varepsilon\right). \tag{11}$$

3.3 L_j subproblem

Although L_j subproblem is nonconvex, we can obtain a suboptimal solution through a local minimization method referred to [4,16,24]. $g(\delta) = w_i^{t+1}\delta_i^p(L_j)\left(1 - \delta_i\left(\left(B_j^{t+1}\right)^T A_j^{t+1}\right)\right)$ can be approximated using first-order Taylor expansion.

$$g(\delta) = g(\delta^k) + \left\langle \nabla g\left(\delta^k\right), \delta - \delta^k \right\rangle. \tag{12}$$

Suppose $\delta^{t+1,k} = \delta\left(L_j^{t+1,k}\right)$ is the k-th iteration solution. Therefore, neglecting the constant term, Eq. (12) can be solved with by iteratively computing

$$L_j^{t+1,k+1} =$$
$$\underset{L_j}{\arg\min} \sum_{i=1}^{\min(d,h)} w_i^{t+1} p\left(\delta_i^k\right)^{p-1}\left(1 - \delta_i\left(\left(B_j^{t+1}\right)^T A_j^{t+1}\right)\right)\delta_i + \beta\left\|R_j x^t - L_j\right\|_F^2 . \tag{13}$$

Equation (13) denotes the weighted nuclear norm and has an analytical solution [4,16,24].

3.4 x Subproblem

Equation (9) is a quadratic problem and has a closed-form solution.

$$x^{s+1} = \left(\Phi^T\Phi + \lambda\beta\sum_j R_j^T R_j\right)^{-1}\left(\Phi^T y + \lambda\beta\sum_j R_j^T L_j^{t+1}\right). \tag{14}$$

When an estimated image x is obtained, the variables w_j, A_j, B_j and L_j can be updated. Then L_j is used to obtain a better estimated image. This process continues to iterate until convergence. The algorithm is summarized as bellows.

Algorithm 1. Image Recovery via Truncated Weighted Schatten-p Norm Regularization

---

Input: an initial image x^0 (DCT based CS method), λ, β, $p = 0.6$, $r = 4$;
    while stopping criteria unsatisfied *do*
        (a) constructing group matrix $R_j x^t$: grouping several similar blocks for x_j^t;
        (b) solving $\{A_j, B_j\}$ subproblem via Eq. (10);
        (c) solving w_j subproblem via Eq. (11);
        (d) solving L_j subproblem via Eq. (13);
        (e) solving x_j subproblem via Eq. (14);
    end while
**Output:** final reconstructed image $\hat{x}$.

---

4   Experimental Results

In order to prove the effectiveness of our model, TWSP is compared with total variation based method (TV) [25], low-rank regularization based method (NLR) [16], weighted nuclear norm based method (WNN) [22] and truncated schatten-p norm based method (TSPN) [24]. Note that TV exploits the gradient sparsity; NLR, WNN and TSPN all employ nonconvex substitution function to exploit nonlocal low-rank property; TSPN shows the current state-of-the-art performance.

The parameters are set as follows: random sampling rate is $\frac{100m}{n}\%$; the size of block is 6×6 and the number of similar blocks is 45; we divide the image into overlapping blocks into reference blocks for every five pixels; the regularization parameter p is 0.6, r is 4, λ and β are tuned separately for each sampling rate. Eight test natural images are used which are shown in Fig. 1. The Peak Signal-to-Noise Ratio (PSNR) is employed to evaluate the different recovery results.

4.1   Experiments on Noiseless Measurements

The PSNR comparison when the sampling rates are 2.5%, 5%, 10%, 15% and 20% is provided in Table 1. From Table 1, we can see that (1) WNN, TSPN and TWSP outperform NLR for almost all the situations; (2) on average, WNN and TSPN get similar recovery results; (3) TWSP obtains the highest PSNRs in all the cases; (4) The average PSNR gains of TWSP over TV, NLR, WNN and TSPN are 3.66 dB, 1.57 dB, 0.39 dB and 0.36 dB respectively with 2.5% sampling rate. The visual results of three images are provided as Figs. 2, 3, and 4. We can see that TWSP can better exploit the nonlocal low-rank property and shows better performance than NLR, WNN and TSPN.

(a)	(b)	(c)	(d)
(e)	(f)	(g)	(h)
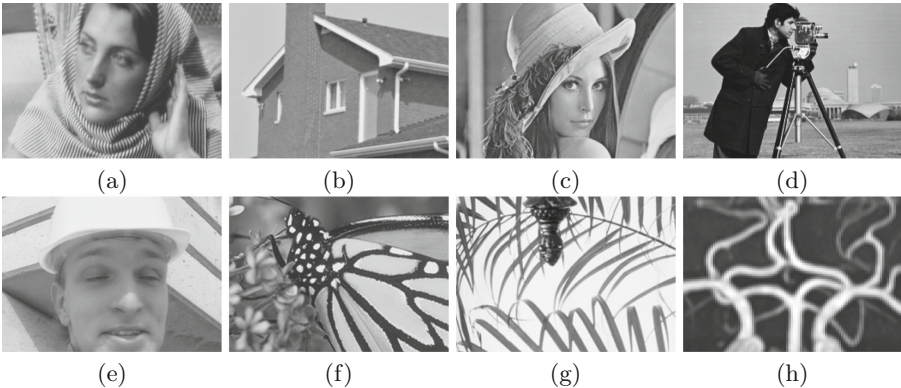
Fig. 1. Eight test images. (a) Barbara; (b) House; (c) Lena; (d) Cameraman; (e) Foreman; (f) Monarch; (g) Leaves; (h) Vessels.

**Table 1.** The PSNR (dB) results on noiseless measurements

Image	Method	Sampling Rate				
		2.5%	5.0%	10%	15%	20%
Barbara	TV	21.56	22.79	24.78	26.72	28.87
	NLR	24.25	29.79	35.47	38.17	40.00
	WNN	25.02	30.54	35.67	38.26	40.13
	TSPN	24.98	30.63	35.64	38.17	40.06
	TWSP	25.21	30.81	35.85	38.40	40.38
House	TV	29.31	30.50	33.63	35.54	37.20
	NLR	32.43	34.80	38.39	40.62	42.49
	WNN	33.20	35.13	38.72	40.77	42.63
	TSPN	33.04	35.08	38.73	40.84	42.62
	TWSP	33.37	35.22	38.81	40.95	42.78
Lena	TV	25.02	26.48	29.63	32.32	34.74
	NLR	26.84	30.69	35.75	38.95	41.38
	WNN	27.55	31.15	35.95	39.09	41.47
	TSPN	27.52	31.26	36.08	39.17	41.44
	TWSP	27.76	31.48	36.31	39.40	41.69
Cameraman	TV	22.16	25.09	28.63	31.48	34.20
	NLR	24.72	28.36	32.30	36.10	39.16
	WNN	25.66	28.67	32.38	36.18	39.29
	TSPN	25.61	28.68	32.67	36.21	39.33
	TWSP	25.91	28.95	32.94	36.50	39.72
Foreman	TV	30.21	32.50	36.02	38.34	40.49
	NLR	33.34	35.70	39.39	41.98	44.02
	WNN	34.63	36.82	39.85	42.34	44.38
	TSPN	34.56	36.87	40.07	42.52	44.49
	TWSP	34.80	37.15	40.29	42.86	44.81
Monarch	TV	20.93	24.21	28.78	31.93	34.84
	NLR	23.76	28.85	34.30	37.78	40.31
	WNN	24.91	29.19	34.44	37.95	40.42
	TSPN	24.74	29.23	34.46	37.86	40.16
	TWSP	25.32	29.36	34.68	38.32	40.82
Leaves	TV	18.23	21.53	25.89	30.03	32.35
	NLR	18.24	27.14	33.80	38.26	41.51
	WNN	20.87	27.66	34.14	38.60	41.96
	TSPN	21.27	27.33	33.87	38.34	41.49
	TWSP	21.56	27.92	34.12	38.86	42.31
Vessels	TV	17.20	20.18	25.03	29.04	32.19
	NLR	17.80	26.09	32.82	37.97	40.95
	WNN	18.96	26.74	33.41	38.11	41.19
	TSPN	19.30	26.56	33.01	38.00	41.48
	TWSP	20.02	27.31	33.94	38.56	42.05
Average	TV	23.08	25.41	29.05	31.93	34.36
	NLR	25.17	30.18	35.28	38.73	41.23
	WNN	26.35	30.74	35.57	38.91	41.43
	TSPN	26.38	30.71	35.57	38.89	41.38
	TWSP	**26.74**	**31.03**	**35.87**	**39.23**	**41.82**

Fig. 2. Recovered Barbara with 5% sampling rate. (a) Original image; (b) NLR recovery (29.79 dB); (c) WNN recovery (30.54 dB); (d) TSPN recovery (30.63 dB); (e) TWSP recovery (30.81 dB).

Fig. 3. Recovered Monarch with 2.5% sampling rate. (a) Original image; (b) NLR recovery (23.76 dB); (c) WNN recovery (24.91 dB); (d) TSPN recovery (24.74 dB); (e) TWSP recovery (25.32 dB).
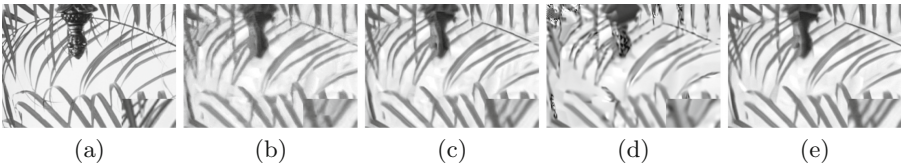
Fig. 4. Recovered Leaves with 2.5% sampling rate. (a) Original image; (b) NLR recovery (18.24 dB); (c) WNN recovery (20.87 dB); (d) TSPN recovery (21.27 dB); (e) TWSP recovery (21.56 dB).

4.2 Experiments on Noisy Measurements

In this subsection, experiments with noisy measurements are carried out to verify the robustness of TWSP approach to Gaussian White noise. The sampling rate is 20%. The signal-to-noise ratio ($SNR = 20 * \log \frac{\bar{A}}{\bar{D}}$), where $\bar{A}$ is the average value and $\bar{D}$ is the standard derivation of noise, varies from 15dB to 35 dB. The PSNR comparisons when SNR is 15 dB, 20 dB, 25 dB, 30 dB and 35 dB are provided in Table 2. TWSP achieves the highest PSNR results among all the methods. The average PSNR gains of TWSP over TV, NLR, WNN and TSPN can be as much as 5.07 dB, 2.80 dB, 1.80 dB and 1.82 dB respectively when SNR=15dB. Some visual results are shown in Figs. 5, 6 and 7, which verify the superiority of our proposed TWSP approach.

Table 2. The PSNR (dB) results of different methods on noisy measurements

Image	Method	SNR				
		15dB	20dB	25dB	30dB	35dB
Barbara	TV	20.91	24.56	28.13	32.79	34.31
	NLR	22.90	26.91	30.42	35.66	37.56
	WNN	23.86	28.43	31.86	36.85	38.26
	TSPN	23.80	28.35	32.00	36.41	37.82
	TWSP	25.64	30.24	33.93	37.80	38.65
House	TV	20.31	24.71	28.87	33.45	36.75
	NLR	23.24	27.98	32.47	35.95	39.64
	WNN	23.61	28.47	33.01	36.71	39.89
	TSPN	23.67	28.53	32.96	36.48	39.77
	TWSP	25.58	30.50	35.11	38.56	41.14
Lena	TV	21.31	24.56	29.30	33.03	34.62
	NLR	23.35	27.59	32.08	36.30	38.43
	WNN	23.93	28.43	33.17	37.21	38.88
	TSPN	23.87	28.34	32.95	36.84	38.63
	TWSP	25.87	30.54	35.44	38.94	40.08
Cameraman	TV	20.14	23.46	27.19	30.49	32.34
	NLR	23.21	26.74	29.85	33.89	35.77
	WNN	23.92	28.32	32.18	35.58	37.04
	TSPN	23.91	28.30	31.90	35.27	36.79
	TWSP	25.88	30.46	34.31	37.22	38.11
Foreman	TV	18.07	22.49	27.59	32.12	35.81
	NLR	22.24	26.02	29.99	35.47	40.52
	WNN	22.81	27.65	32.43	37.16	41.72
	TSPN	22.78	27.58	32.37	36.96	41.37
	TWSP	24.66	29.54	34.50	39.27	42.43
Monarch	TV	21.42	25.01	28.17	31.15	32.01
	NLR	23.33	27.15	30.95	35.42	37.58
	WNN	24.40	28.65	32.79	36.59	38.16
	TSPN	24.33	28.55	32.28	36.00	37.81
	TWSP	26.24	30.69	34.83	38.01	39.00
Leaves	TV	17.89	21.86	24.83	27.55	30.42
	NLR	19.01	22.63	26.26	31.58	35.80
	WNN	20.38	24.70	29.06	33.85	36.73
	TSPN	20.49	24.83	28.92	33.43	36.32
	TWSP	21.85	26.16	30.68	35.69	38.29
Vessels	TV	22.86	27.03	29.44	31.27	32.30
	NLR	23.78	27.99	33.12	37.85	39.93
	WNN	26.14	30.50	35.06	38.28	40.46
	TSPN	26.03	30.40	34.65	38.09	40.24
	TWSP	27.73	32.83	37.40	39.83	40.79
Average	TV	20.36	24.21	27.94	31.48	33.57
	NLR	22.63	26.63	30.64	35.27	38.15
	WNN	23.63	28.14	32.45	36.53	38.89
	TSPN	23.61	28.11	32.25	36.19	38.59
	TWSP	**25.43**	**30.12**	**34.53**	**38.17**	**39.81**

Fig. 5. Recovered Cameraman with SNR = 35 dB. (a) Original image; (b) NLR recovery (35.77 dB); (c) WNN recovery (37.04 dB); (d) TSPN recovery (36.99 dB); (e) TWSP recovery (38.11 dB).

Fig. 6. Recovered Foreman with SNR = 30 dB. (a) Original image; (b) NLR recovery (35.47 dB); (c) WNN recovery (37.16 dB); (d) TSPN recovery (36.96 dB); (e) TWSP recovery (39.27 dB).
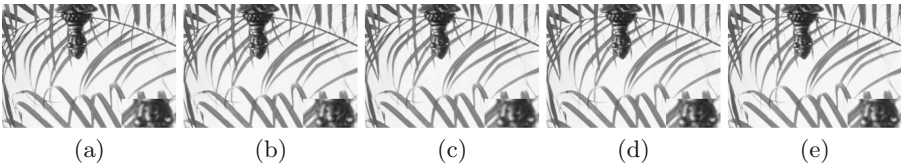
Fig. 7. Recovered of Leaves with SNR = 35 dB. (a) Original image; (b) NLR recovery (35.80 dB); (c) WNN recovery (36.73 dB); (d) TSPN recovery (36.32 dB); (e) TWSP recovery (38.29 dB).

5   Conclusion

In this paper, we have presented a new approach toward image recovery via truncated weighted schatten-p norm which is taking advantages of both weighted nuclear norm and truncated schatten-p norm. Truncated weighted schatten-p norm can better exploit the nonlocal low-rank property than current CS methods based on low-rank regularization. In addition, we also propose an efficient iterative scheme based on alternating direction method of multipliers to accurately solve the nonconvex optimization model. Experimental results demonstrate that our proposed algorithm is exceeding the existing state-of-the-art methods, in terms of subjective and objective qualities.

References

1. Donoho, D.L.: Compressed sensing. IEEE Trans. Inf. Theory **52**, 1289–1306 (2006)
2. Cand, E.J., Wakin, M.B.: "people hearing without listening:" an introduction to compressive sampling. IEEE Signal Process. Mag. **25**, 21–30 (2008)
3. Feng, L., Sun, H.: Blind compressive sensing method via local sparsity and nonlocal similarity. J. Nanjing Univ. Sci. Technol. **41**, 399–404 (2017)
4. Feng, L., Sun, H., Sun, Q., Xia, G.: Compressive sensing via nonlocal low-rank tensor regularization. Neurocomputing **216**, 45–60 (2016)
5. Zou, X., Feng, L., Sun, H.: Robust compressive sensing of multichannel eeg signals in the presence of impulsive noise. Inf. Sci. **429**, 120–129 (2018)
6. Zhang, J., Zhao, D., Zhao, C., Xiong, R., Ma, S., Gao, W.: Compressed sensing recovery via collaborative sparsity. In: Data Compression Conference, pp. 287–296 (2012)
7. Yao, X., Han, J., Zhang, D., Nie, F.: Adaptively determining regularization parameters in non-local total variation regularization for image denoising. Electron. Lett. **51**, 144–145 (2015)
8. Bioucas-Dias, J.M., Figueiredo, M.A.T.: A new twist: Two-step iterative shrinkage/thresholding algorithms for image restoration. IEEE Trans. Image Process. **16**, 2992 (2007)
9. Becker, S., Bobin, J., Cands, E.J.: Nesta: A fast and accurate first-ordermethod for sparse recovery. SIAM J. Imaging Sci. **4**, 1–39 (2009)
10. Javaherian, A., Soleimani, M., Moeller, K., Movafeghi, A., Faghihi, R.: An accelerated version of alternating direction method of multipliers for tv minimization in eit. Appl. Math. Model. **40**, 8985–9000 (2016)
11. Bertalmio, M., Caselles, V., Roug, B., Sol, A.: Tv based image restoration with local constraints. J. Sci. Comput. **19**, 95–122 (2003)
12. Wang, Y.C.F., Wei, C.P., Chen, C.F.: Low-rank matrix recovery with structural incoherence for robust face recognition. In: Computer Vision and Pattern Recognition, pp. 2618–2625 (2012)
13. Wei, C.P., Chen, C.F., Wang, Y.C.F.: Robust face recognition with structurally incoherent low-rank matrix decomposition. IEEE Trans. Image Process. **23**, 3294–3307 (2014)
14. Nguyen, H., Yang, W., Shen, F., Sun, C.: Kernel low-rank representation for face recognition. Neurocomputing **155**, 32–42 (2015)
15. Han, J., Quan, R., Zhang, D., Nie, F.: Robust Object Co-Segmentation Using Background Prior. IEEE Trans. Image Process. **27**, 1639–1651 (2018)
16. Dong, W., Shi, G., Li, X., Ma, Y.: Compressive sensing via nonlocal low-rank regularization. IEEE Trans. Image Process. **23**, 3618–3632 (2014)
17. Wang, H., Zhao, R., Cen, Y.: Rank adaptive atomic decomposition for low-rank matrix completion and its application on image recovery. Neurocomputing **145**, 374–380 (2014)

18. Cabral, R., Torre, F.D.L., Costeira, J.P., Bernardino, A.: Unifying nuclear norm and bilinear factorization approaches for low-rank matrix decomposition. In: IEEE International Conference on Computer Vision, pp. 2488–2495 (2014)
19. Toh, K.C., Yun, S.: An accelerated proximal gradient algorithm for nuclear norm regularized least squares problems. Pac. J. Optim. **6**, 615–640 (2009)
20. Wang, J., Wang, M., Hu, X., Yan, S.: Visual data denoising with a unified schatten-p norm and lq norm regularized principal component pursuit. Pattern Recognit. **48**, 3135–3144 (2015)
21. Cai, J.F., Candes, E.J., Shen, Z.: A singular value thresholding algorithm for matrix completion. SIAM J. Optim. **20**, 1956–1982 (2008)
22. Gu, S., Zhang, L., Zuo, W., Feng, X.: Weighted nuclear norm minimization with application to image denoising. In: IEEE Conference on Computer Vision and Pattern Recognition, pp. 2862–2869 (2014)
23. Xie, Y., Gu, S., Liu, Y., Zuo, W., Zhang, W., Zhang, L.: Weighted schatten p-norm minimization for image denoising and background subtraction. IEEE Trans. Image Process. **25**, 4842–4857 (2015)
24. Feng, L., Sun, H., Sun, Q., Xia, G.: Image compressive sensing via truncated schatten-p norm regularization. Signal Process. Image Commun. **47**, 28–41 (2016)
25. Zhang, J., Liu, S., Xiong, R., Ma, S., Zhao, D.: Improved total variation based image compressive sensing recovery by nonlocal regularization. In: IEEE International Symposium on Circuits and Systems, pp. 2836–2839 (2013)